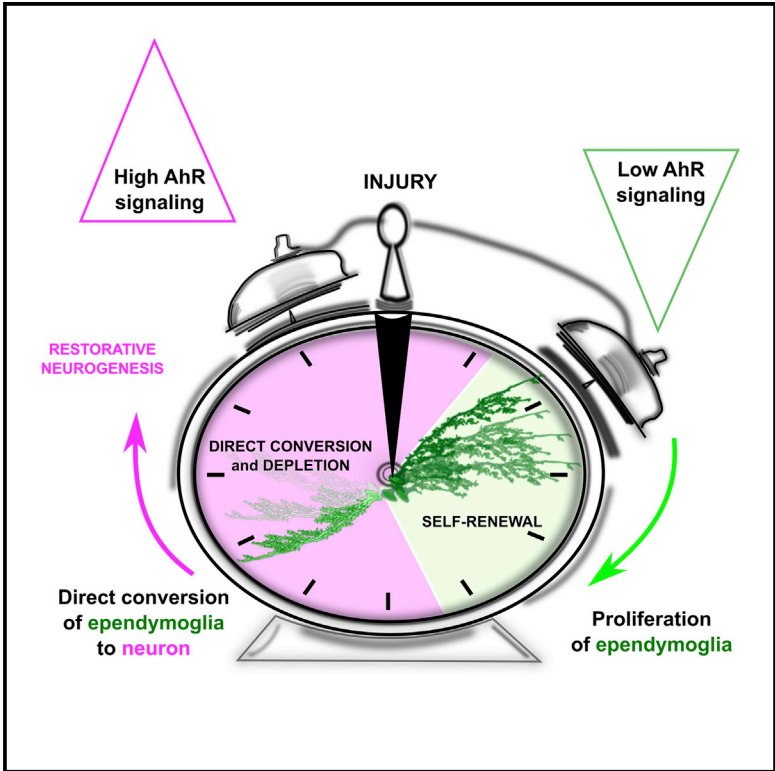# The Aryl Hydrocarbon Receptor Pathway Defines the Time Frame for Restorative Neurogenesis

Graphical Abstract

Authors

Rossella Di Giaimo, Tamara Durovic, Pablo Barquin, ..., Wolfgang Wurst, Stefan H. Stricker, Jovica Ninkovic

Correspondence

ninkovic@helmholtz-muenchen.de

In Brief

Zebrafish have a high capacity to replace lost neurons after brain injury. Di Giaimo et al. identify the aryl hydrocarbon receptor (AhR) as a crucial regulator of restorative neurogenesis timing in the zebrafish brain. Interference with timely AhR regulation after injury leads to aberrant restorative neurogenesis.

Highlights

- Aryl hydrocarbon receptor (AhR) pathway is crucial for brain regeneration

- High AhR levels promote conversion of ependymoglia to neurons during regeneration

- Low AhR levels promote ependymoglial proliferation in the injured brain

- AhR levels set the proper timing of restorative neurogenesis

Report

The Aryl Hydrocarbon Receptor Pathway Defines the Time Frame for Restorative Neurogenesis

Rossella Di Giaimo,[1,2,17] Tamara Durovic,[1,3,17] Pablo Barquin,[4] Anita Kociaj,[1,3] Tjasa Lepko,[1,3] Sven Aschenbroich,[1,3]
Christopher T. Breunig,[5,6] Martin Irmler,[7] Filippo M. Cernilogar,[8] Gunnar Schotta,[8,9] Joana S. Barbosa,[1,18]
Dietrich Trümbach,[10] Emily Violette Baumgart,[1] Andrea M. Neuner,[5,6] Johannes Beckers,[7,11,12] Wolfgang Wurst,[10,13,14,15]
Stefan H. Stricker,[5,6] and Jovica Ninkovic[1,16,19,*]
[1]Institute of Stem Cell Research, Helmholtz Center Munich, 85764 Neuherberg, Germany
[2]Department of Biology, University of Naples Federico II, 80134 Naples, Italy
[3]Graduate School of Systemic Neurosciences, Biomedical Center of LMU, 82152 Planegg, Germany
[4]Universidad Pablo de Olavide, Sevilla, 41013 Sevilla, Spain
[5]MCN Junior Research Group, Munich Center for Neurosciences, 82152 Munich, Germany
[6]Epigenetic Engineering, Institute of Stem Cell Research, Helmholtz Center Munich, 85764 Neuherberg, Germany
[7]Institute of Experimental Genetics, Helmholtz Zentrum München, 85764 Neuherberg, Germany
[8]Division of Molecular Biology, Biomedical Center, Faculty of Medicine, LMU Munich, 82152 Planegg, Germany
[9]Munich Center for Integrated Protein Science (CiPSM), 82152 Planegg, Germany
[10]Institute of Developmental Genetics, Helmholtz Zentrum München, 85764 Neuherberg, Germany
[11]German Center for Diabetes Research (DZD), 85764 Neuherberg, Germany
[12]Technische Universität München, Chair of Experimental Genetics, 85354 Freising-Weihenstephan, Germany
[13]Munich Cluster for Systems Neurology SYNERGY, 82152 Planegg, Germany
[14]German Center for Neurodegenerative Diseases (DZNE), 82152 Planegg, Germany
[15]Chair of Developmental Genetics, Technische Universität München, 85354 Freising-Weihenstephan, Germany
[16]Department for Cell Biology and Anatomy, Biomedical Center of LMU, 82152 Planegg, Munich, Germany
[17]These authors contributed equally
[18]Present address: Institute of Animal Pathology, Vetsuisse Faculty, University of Bern, Bern, Switzerland
[19]Lead Contact
*Correspondence: ninkovic@helmholtz-muenchen.de
https://doi.org/10.1016/j.celrep.2018.11.055

SUMMARY

Zebrafish have a high capacity to replace lost neurons after brain injury. New neurons involved in repair are generated by a specific set of glial cells, known as ependymoglial cells. We analyze changes in the transcriptome of ependymoglial cells and their progeny after injury to infer the molecular pathways governing restorative neurogenesis. We identify the aryl hydrocarbon receptor (AhR) as a regulator of ependymoglia differentiation toward post-mitotic neurons. *In vivo* imaging shows that high AhR signaling promotes the direct conversion of a specific subset of ependymoglia into post-mitotic neurons, while low AhR signaling promotes ependymoglial proliferation. Interestingly, we observe the inactivation of AhR signaling shortly after injury followed by a return to the basal levels 7 days post injury. Interference with timely AhR regulation after injury leads to aberrant restorative neurogenesis. Taken together, we identify AhR signaling as a crucial regulator of restorative neurogenesis timing in the zebrafish brain.

INTRODUCTION

Regeneration in the mammalian CNS is largely limited (Dimou and Götz, 2014) and restricted to either demyelinated axon

repair (Dimou and Götz, 2014) or, in very few cases, neuronal repair (Arvidsson et al., 2002; Chen et al., 2004; Ernst et al., 2014). Neuronal replacement in mammals is limited to brain areas in close proximity to neurogenic zones (Brill et al., 2009). However, a large number of young neurons originating from the neurogenic zones fail to mature and integrate at the injury site and instead die (Arvidsson et al., 2002; Brill et al., 2009). In contrast, the zebrafish CNS has the capacity to regenerate brain tissue after injury (Becker and Becker, 2015). This regeneration also includes the replacement of lost neurons (restorative neurogenesis) (Barbosa et al., 2015; Baumgart et al., 2012; Kishimoto et al., 2012; Kroehne et al., 2011; Kyritsis et al., 2012). Tremendous regeneration capacity coincides with the wide spread of ependymoglial cells producing different neuronal subtypes in the zebrafish brain throughout their lifetime (Kyritsis et al., 2012). Notably, ependymoglial cells lining the ventricular surface in the adult zebrafish telencephalon generate new neurons that are recruited to the injury site (Barbosa et al., 2015; Baumgart et al., 2012; Kishimoto et al., 2012; Kyritsis et al., 2012). Importantly, a considerable proportion of these additionally generated neurons fully differentiate into the appropriate neuronal subtypes and survive for more than 3 months (Baumgart et al., 2012; Kroehne et al., 2011). The activation of ependymoglial cells to produce additional neurons is preceded by the activation of microglial cells involved in the initial wound healing process. Importantly, the initial inflammation does not only remove cellular debris but also induces restorative neurogenesis (Kyritsis et al., 2012), suggesting a biphasic regeneration process in the zebrafish brain. During the first phase, activated glial cells restrict the
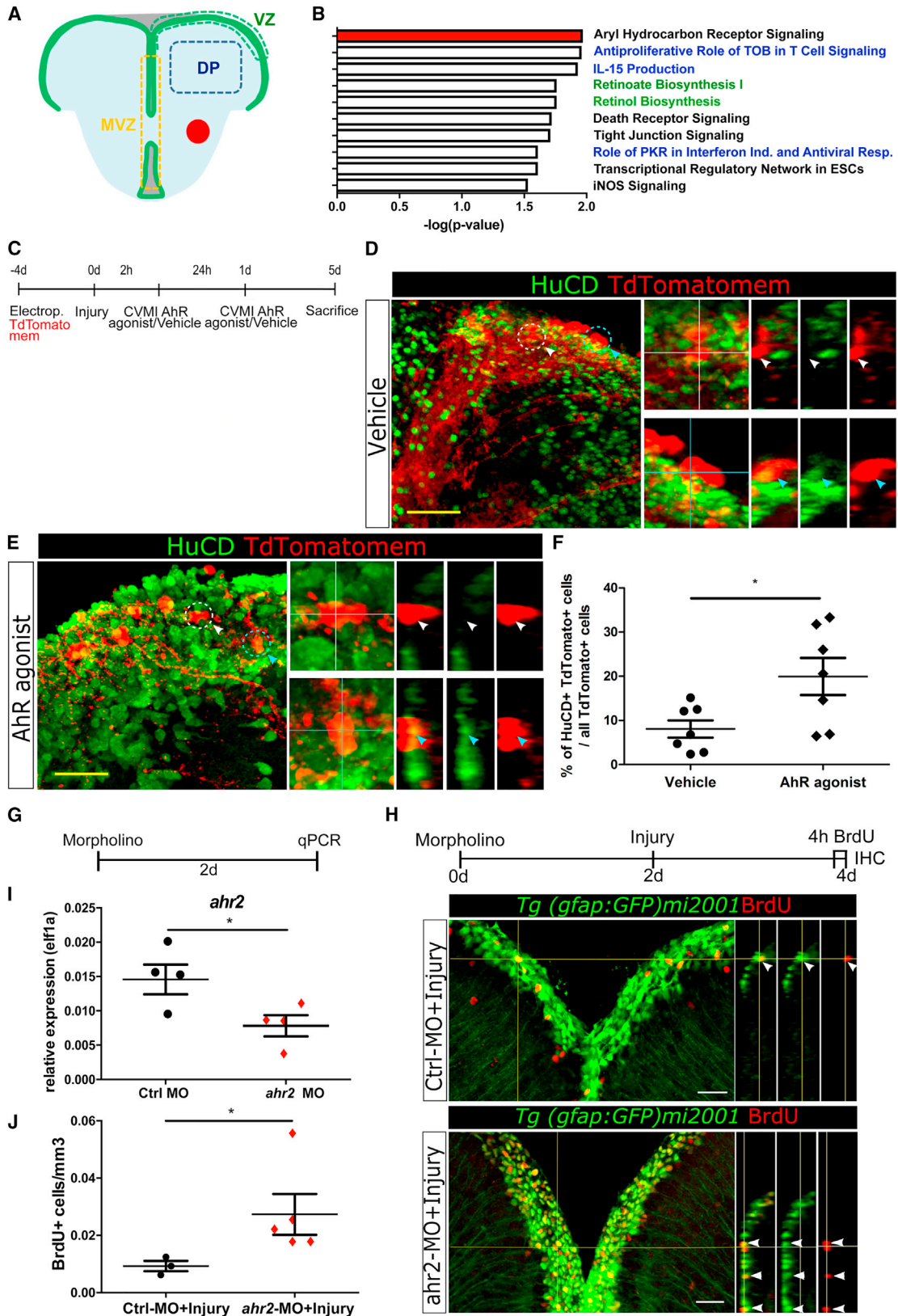
(legend on next page)

initial damage and clear cellular debris. The following second phase promotes the production of new neurons from the ependymoglia that are necessary for tissue restoration (Kyritsis et al., 2012). This delay in restorative neurogenesis relative to the initial inflammatory phase therefore stands as a crucial mechanism to allow correct zebrafish brain regeneration. For this reason, understanding the specific molecular programs underlying the timely production of new neurons is critical to implement regeneration from endogenous glial cells in the mammalian brain. Despite their importance, these mechanisms, which are involved in the temporal control of restorative neurogenesis from ependymoglial cells, are not well understood. Therefore, we aim to identify them using both longitudinal analysis of injury-induced transcriptome changes in ependymoglial niches and the cell-type-specific manipulation of these pathways.

RESULTS

To define the molecular pathways controlling restorative neurogenesis initiation in the dorsal neurogenic zone (VZ) of the zebrafish telencephalon (Barbosa et al., 2015), we aimed to identify injury-induced changes in the transcriptome specific for the VZ. To this end, we compared changes in the transcriptome in laser-dissected tissue from 3 different telencephalic areas from intact and stab-wound injured brains (Barbosa et al., 2016) using the Affymetrix Zebrafish Gene 1.x ST array (Figure 1A). We compared injury-induced changes in the VZ to changes in the brain parenchyma (DP), which is free of neuronal progenitors, to reveal a signature specific for this cell type. Moreover, a comparison with the medial neurogenic zone (MVZ) was performed to extract pathways specific for progenitors in the VZ engaged in the repair process. Non-supervised hierarchical clustering of injury-induced changes at 2 and 7 days after injury in these 3 different areas revealed several clusters of co-regulated genes. These clusters were either specific to the VZ (clusters 1 and 2), shared between neurogenic niches (clusters 3 and 4), or changed in all 3 analyzed areas (clusters 5 and 6; Figures S1A and S1B; Table S1). We reasoned that the molecular signature controlling the early response of the ependymoglia should be upregulated specifically in the dorsal neurogenic zone at 2 dpi, correlating with the first signs of ependymoglia reaction

to injury (Baumgart et al., 2012), and should chase out at 7 dpi, as represented by cluster 1 (Figure S1A). We observed 192 genes specifically upregulated in the VZ at 2 dpi (Figure S1B). Ingenuity Pathway Analysis (IPA) of these genes revealed significant over-representation of several metabolic (green) and immune-system-related (blue) pathways (Figure 1B; Table S1). However, the most significantly regulated pathway was the aryl hydrocarbon receptor (AhR) signaling pathway (Figure 1B), placing it as our prime candidate for further analysis. We therefore analyzed the expression of AhR-signaling-regulated genes after injury and observed an upregulation of Irf9, Nfkbie, and Tgfb1 specifically at 2 dpi (Figure S1C), which was indicative of reduced AhR signaling. Taken together, our data revealed a specific inhibition of AhR signaling in the dorsal neurogenic zone at 2 dpi that then chases out at 7 dpi, suggesting its role in the initial control of restorative neurogenesis.

To address the importance of AhR signaling levels in restorative neurogenesis, we either potentiated AhR signaling with a high-affinity AhR agonist, β-naphthoflavone (BNF; Berghard et al., 1992), or decreased it by morpholino-mediated knockdown. AhR is a ligand-dependent transcription factor that is restrained in the cytoplasm by a chaperone complex when inactive (Hestermann and Brown, 2003). Upon ligand binding, AhR translocates to the nucleus and activates the transcription of its downstream targets (Hestermann and Brown, 2003). BNF induces AhR translocation to the nucleus without a natural ligand and therefore activates AhR signaling (Soshilov and Denison, 2014). To minimize systemic effects, we injected 10 μg/g of body mass of BNF in the telencephalic ventricle using cerebroventricular microinjections (CVMIs) (Figure 1C). We first analyzed the efficiency of CVMI-administered BNF to activate AhR signaling based on the expression levels of cytochrome P450 1B1 oxidase (Cyp1b1), a transcriptional reporter for AhR signaling (Soshilov and Denison, 2014). Notably, we detected more than 2-fold higher levels of Cyp1b1 in the injured brains in BNF-treated animals compared to the vehicle treatment (Figure S1D). We then assessed the number of new neurons generated from ependymoglial cells (Figures 1C–1F). To follow both ependymoglia and their progeny, including newly generated neurons, we labeled ependymoglia by electroporation of a plasmid encoding for membrane-localized TdTomato

Figure 1. Levels of AhR Signaling Define the Balance between Ependymoglial Proliferation and Differentiation

(A) Schematic representation of the laser-microdissected areas used for transcriptome analysis.

(B) Histogram depicting canonical pathways (Ingenuity) enriched in the gene set specifically upregulated in the dorsal VZ at 2 dpi.

(C) Scheme showing the experimental outline to assess the influence of AhR potentiation on restorative neurogenesis.

(D and E) Confocal images showing the fate of TdTomatomem-labeled cells in AhR agonist-treated (E) and vehicle-treated (D) brains 5 days after injury. High magnification images with orthogonal projections depict representative TdTomatomem+/HuC/D− (white circle) and TdTomatomem/HuC/D double-positive (blue circle) cells. White arrowhead indicates HuC/D-negative and blue arrowhead HuC/D-positive cells. Scale bars, 50 μm.

(F) Dot plot showing the proportion of HuC/D and TdTomatomem double-positive cells among all TdTomatomem-labeled cells in AhR agonist- and vehicle-treated brain.

(G) Scheme depicting the experimental procedure to assess the efficiency of morpholino-mediated AhR knockdown in ependymoglia.

(H) Scheme of the experimental procedure used to analyze ependymoglia proliferation after morpholino-mediated knockdown and confocal images with orthogonal projections showing examples of proliferating, BrdU-positive ependymoglia (white arrowhead) in the injured brains after control or ahr2-specific morpholino treatment. Scale bars, 20 μm.

(I) Dot plot showing ahr2 expression in ependymoglia.

(J) Dot plot depicting the number of proliferating ependymoglia after reducing AhR signaling.

Single dots represent individual animals indicating biological replicates in all dot plots. Lines show mean ± SEM. *p ≤ 0.05 (Mann-Whitney test). VZ, dorsal neurogenic zone (50 um width from the ventricular surface); MVZ, medial neurogenic zone; DP, brain parenchyma (DP areas were chosen far from the injury sites [red circle in A]).
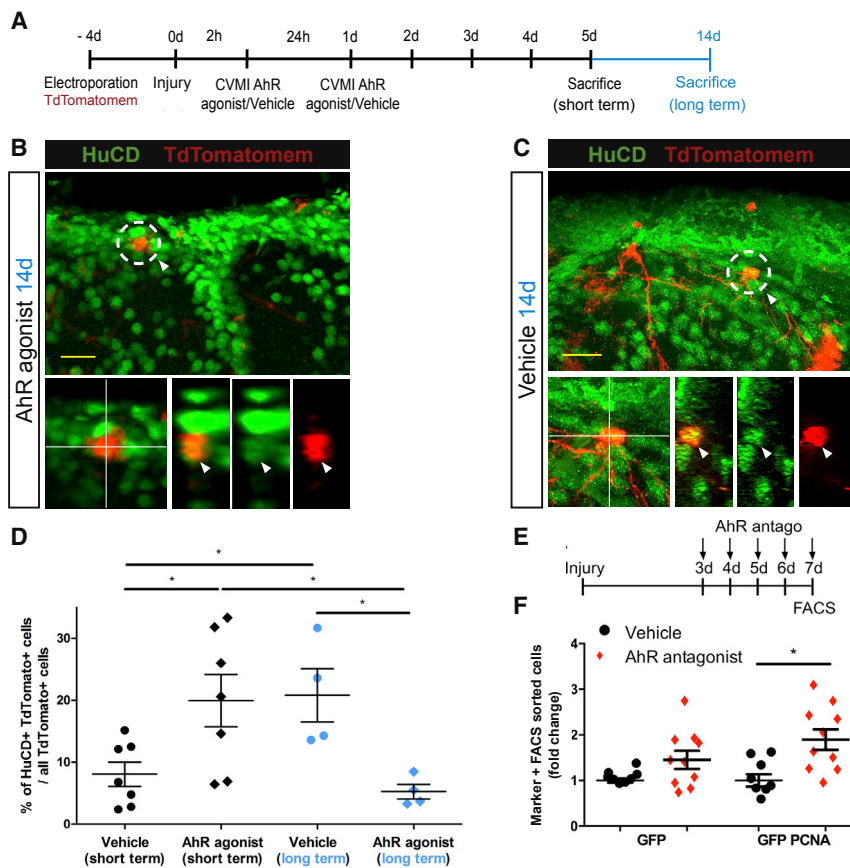
Figure 2. AhR Signaling Regulates the Timing of the Restorative Neurogenesis that Is Crucial for the Survival of Newborn Neurons

(A) Schematic representation of the experimental procedure used to follow ependymoglial progeny after injury and the activation of AhR signaling.

(B and C) Micrographs depicting HuC/D and TdTomatomem double-positive cells without radial morphology in AhR agonist-treated (B) or vehicle-treated (C) brains 14 days after injury. Dashed white circles indicate representative cells that are magnified in the lower panel with orthogonal projections. Images are presented as full z-projections of the confocal z stack. Scale bars, 20 μm.

(D) Dot plot showing the percentage of double-positive HuC/D and TdTomatomem cells among all TdTomatomem-positive cells after treatment with AhR agonist or vehicle at 5 dpi (short term) and 14 dpi (long term).
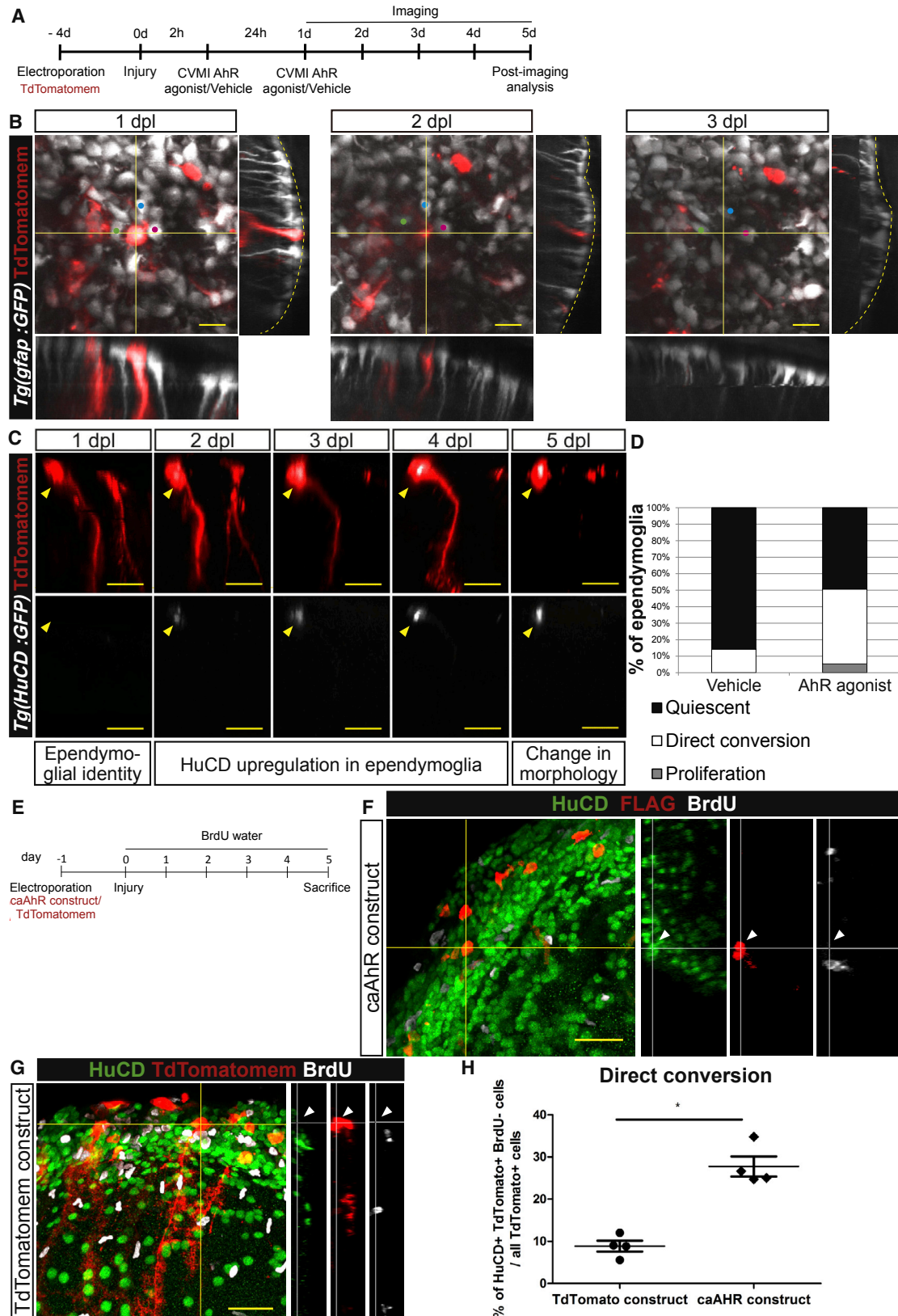
(E) Scheme showing the experimental outline to assess the impact of low AhR levels on ependymoglial proliferation.

(F) Dot plot depicting the change in the number of PCNA-positive ependymoglia in injured telencephalon treated with vehicle or AhR antagonist. Single dots represent individual animals indicating biological replicates in all dot plots. Lines show mean ± SEM. *p ≤ 0.05 (Mann-Whitney test).

rons after AhR potentiation was significantly lower at 14 dpi (long-term tracing, Figure 2D) compared to 5 dpi (Figure 2D), suggesting impaired survival of additional neurons generated due to the inappropriate regulation of AhR signaling. To complement this analysis of precocious activation of AhR signaling, we interfered with the return of AhR signaling to basal levels after the initial decrease following injury and analyzed the proliferation of ependymoglia. To achieve the precise timing of interference with AhR signaling, we used a pharmacological approach and locally administered 6 μM AhR antagonist (AhR Antagonist II, SR1-CAS) using CVMI. Administration of the antagonist efficiently decreased AhR signaling, as measured by Cyp1b1 expression (Figure S2A). AhR levels were then kept low by the daily administration of the agonist starting at day 3 after injury, and the number of actively cycling, PCNA+ ependymoglia was determined at 7 dpi using intracellular fluorescence-activated cell sorting (FACS) (Figures 2E, 2F, and S2C), as previously described (Barbosa et al., 2016). We chose to analyze samples at 7 dpi because this is the time point when the expression of Cyp1b1 is again increased to basal levels observed in the intact brain (Figure 4E). The number of proliferating ependymoglia significantly increased (Figures 2E and 2F) after antagonist treatment compared to the vehicle control. This increase correlates with our hypothesis that low AhR levels allow the proliferation of ependymoglia after injury. Our data, therefore, suggest a role of AhR in regulating the balance between the proliferation and differentiation of ependymoglia to ensure the proper timing of restorative neurogenesis.

(TdTomatomem) red fluorescent protein (Barbosa et al., 2015) (Figure 1C), allowing the long-term tracing of the ependymoglial lineage (Barbosa et al., 2015, 2016). Elevated AhR signaling in the injured brain increased the number of newborn, HuC/D-positive neurons derived from the electroporated ependymoglial cells compared to the vehicle treatment (Figures 1D–1F). Conversely, the morpholino-mediated knockdown of aryl hydrocarbon receptor 2 (ahr2; Figures 1G and 1I), a major mediator of AhR signaling in zebrafish (Bello et al., 2004), increased the ependymoglia proliferation compared to control morpholino (Figures 1H and 1I). Taken together, our data suggest a role for AhR signaling levels in controlling ependymoglial behavior after injury, with high levels of AhR signaling promoting neurogenesis from the zebrafish ependymoglia and low AhR signaling triggering their proliferation and/or self-renewal.

To assess the importance of this regulation, we followed the fate of new neurons added after AhR potentiation using TdTomatomem-based fate mapping. We analyzed the fate of progeny at 5 (short-term tracing) and 14 days (long-term tracing) after injury (Figure 2A). As expected, the proportion of new TdTomatomem+ HuC/D+ neurons significantly increased after AhR potentiation compared to the vehicle-treated animals in short-term tracing. The proportion of TdTomatomem+ and HuC/D+ neurons increased further at 14 days compared to 5 days after vehicle treatment (Figures 2B–2D). Surprisingly, we observed that the number of TdTomatomem+, HuC/D+ neu-

(legend on next page)

Restorative neurogenesis in zebrafish is achieved by both an increase in the number of dividing neuronal progenitors (Barbosa et al., 2015) and an increase in the direct conversion of ependymoglia into post-mitotic neurons (Barbosa et al., 2015). To assess the direct conversion of ependymoglia after injury and AhR signaling activation, we sparsely labeled ependymoglia by the electroporation of TdTomatomem (Barbosa et al., 2015) and followed individual labeled ependymoglia and their progeny for 5 days by live imaging (Figures 3A, 3B, S3A, and S3B). The identity of the followed cells was then assessed by post-imaging staining for neuronal marker HuC/D. This allowed the re-identification of previously imaged cells (Figures S3E–S3G). We electroporated plasmids in the *Tg(gfap:GFP)*mi2001 transgenic line expressing GFP in all ependymoglia (also retained in 25% of their progeny) to identify the ependymoglia identity by GFP expression and the radial morphology, as previously described (Barbosa et al., 2015, 2016). The direct conversion of ependymoglia into neurons was then characterized by the loss of radial morphology, migration out of the ependymoglial layer toward the brain parenchyma (Figures 3B and S3F), and the expression of the post-mitotic marker HuC/D prior to a change in radial morphology (Figure 3C; Figure S3G). In line with our previous observation (Barbosa et al., 2015), only a few ependymoglial cells divided (Figure 3D; Figures S3A and S3B), and the vast majority (85%) of labeled ependymoglia in vehicle-treated injured telencephalons remained quiescent. These ependymoglia cells did not change their identity within a 5-day imaging period (Figures 3D and S3A), whereas 14.2% of labeled cells directly converted (Figures 3B–3D). In contrast, after AhR signaling enhancement, 45% of labeled ependymoglial cells directly converted into post-mitotic neurons (Figure 3D). This increase in direct conversion was associated with the depletion of ependymoglia present in the dorsal neurogenic niche, as we observed a significant increase in the dorsal surface free of gfap:GFP-positive ependymoglia in BNF-treated brains compared to the vehicle treatment (Figures S3H and S3I; Videos S1 and S2). We did not observe any difference in terminal deoxynucleotidyl transferase-mediated deoxyuridine triphosphate nick end labeling (TUNEL)-positive cells at the dorsal telencephalon area between the BNF and vehicle treatment (Figures S3C and S3D). Therefore, we concluded that direct conversion causes ependymoglial depletion rather than cell death. Taken together, our data suggest that AhR signaling enhancement after injury leads to increased neurogenesis via the direct conversion and depletion of ependymoglia.

Restorative neurogenesis in zebrafish is tightly associated with the activation of microglia and monocyte infiltration (Kyritsis et al., 2012), and AhR signaling regulates monocyte extravasation (Rothhammer et al., 2016). Therefore, we next wondered if increased AhR signaling levels would promote the direct conversion of ependymoglia in a cell-autonomous manner. To assess this hypothesis, we potentiated AhR signaling in a cell-autonomous manner by electroporating the constitutively active AhR construct (caAhR) in ependymoglia (Figure S3J). The caAhR construct is generated by fusing the N-terminal portion of zebrafish ahr2 lacking a PAS B domain with the transactivation domain of mouse AhR that activates the canonical AhR pathway independently of the ligand binding (Soshilov and Denison, 2014). We co-electroporated caAhR with TdTomatomem for long-term fate mapping and kept the animals in the BrdU bath to label all dividing cells over a 5-day experiment (Figure 3E). Since the electroporation initially labels virtually only ependymoglia (Figure S3J; see also Barbosa et al., 2015), we reasoned that TdTomatomem+, BrdU+, and post-mitotic neuronal marker HuC/D+ cells represent new neurons being generated from proliferating progenitors, while TdTomatomem+, HuC/D+, and BrdU− cells arose from the direct conversion of ependymoglia without cell division (Figures 3F and 3G). Similar to live imaging, we observed that 10% of cells electroporated with the control plasmid acquired neuronal identity (HuC/D+) without BrdU incorporation. However, the cells electroporated with caAhR showed a 3-fold increase in direct conversions (Figure 3H). All in all, our analysis indicates that the AhR levels regulate the direct conversion of ependymoglia in a cell-autonomous manner.

Increased levels of AhR in the injured brain promoted the direct conversion of up to 45% of all ependymoglia, prompting us to hypothesize that only a subset of ependymoglia respond to the AhR levels in a given condition. Indeed, live imaging of ependymoglia in the *Tg(gfap:GFP)mi2001* transgenic line (Bernardos and Raymond, 2006) revealed two states of gfap:GFP+ ependymoglial cells (GFP^{low} and GFP^{high}) based on the GFP expression levels (Figure 4A). Approximately 25% of the ependymoglial progeny remain GFP+ (Barbosa et al., 2015) due to GFP protein stability. Therefore, to exclude that GFP^{low} state represents ependymoglial progeny, we analyzed the morphology of GFP+ cells in confocal stacks from live imaging and in non-stained

Figure 3. High AhR Signaling Induces Direct Conversion of Ependymoglia into Post-Mitotic Neurons
(A) Schematic representation of the experimental procedure used to follow the cell fate of ependymoglia after injury and the activation of AhR signaling using *in vivo* imaging.
(B) 2-photon images with orthogonal projections of the same TdTomatomem-labeled ependymoglia in a Tg(*gfap:GFP*)mi2001 line followed for 5 days, depicting direct conversion. Yellow line delineates the ventricular surface.
(C) 2-photon images with orthogonal projections of the same TdTomatomem-labeled ependymoglia in the Tg(*HuC:GFP*) line followed for 5 days, depicting different phases of direct conversion including the upregulation of the HuC/D marker.
(D) Histogram representing the behavior of ependymoglial cells in the injured vehicle and AhR agonist-treated brains observed using live imaging.
(E) Schematic representation of the experimental procedure used to follow direct conversion after cell-autonomous enhancement of AhR signaling in the injured brains.
(F and G) Micrographs with orthogonal projections depicting the fate of ependymoglial progeny after caAhR construct (F) or TdTomatomem control construct (G) electroporation at 5 days after brain injury.
(H) Dot plot showing the percentage of ependymoglial direct conversion (HuC/D and TdTomatomem double-positive cells negative for BrdU) after caAHR for TdTomatomem construct electroporation. Single dots represent individual animals indicating biological replicates. Lines show mean ± SEM. *p ≤ 0.05 (Mann-Whitney test). Scale bars, 30 μm.
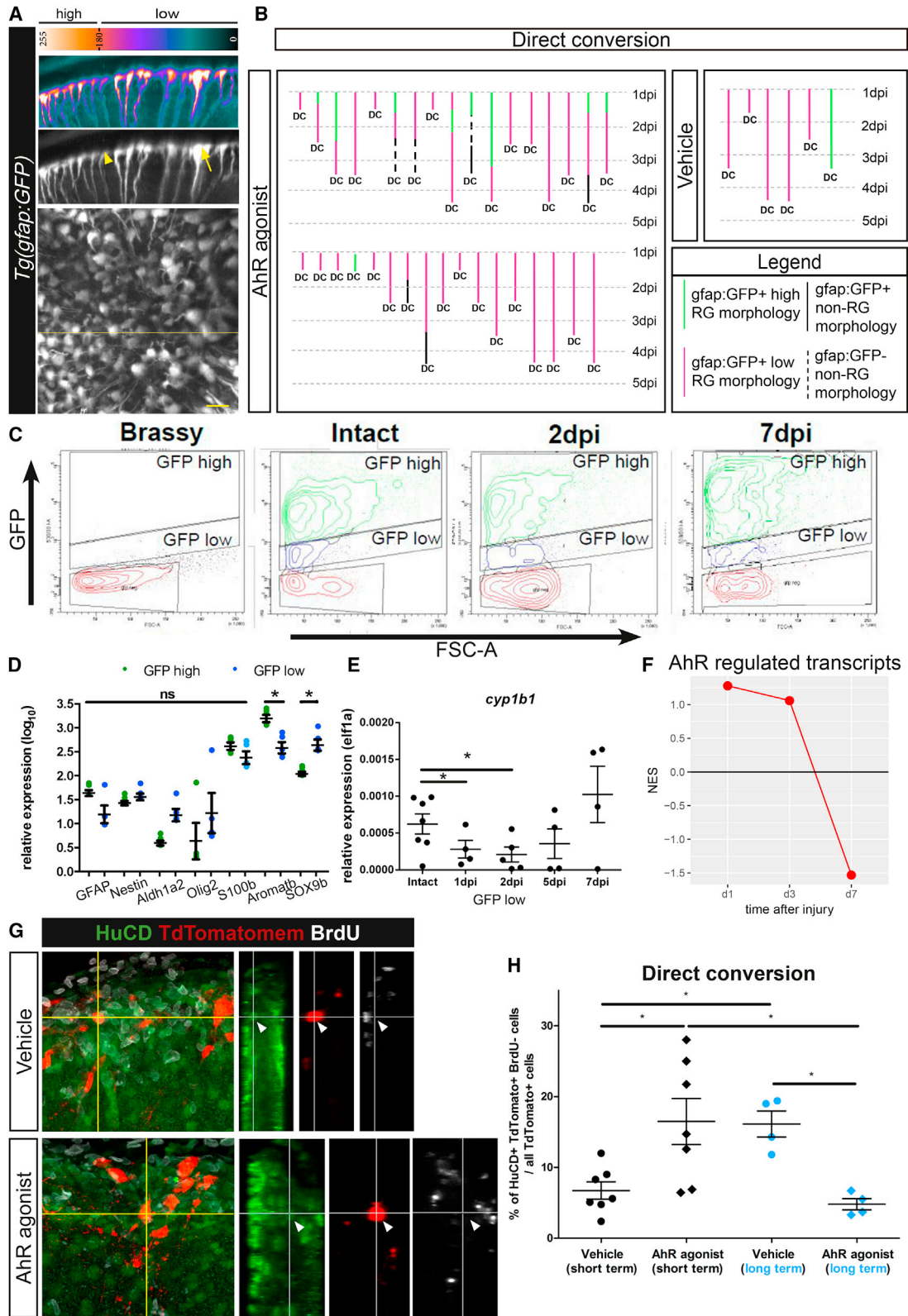
(legend on next page)

brain sections of the dorsal VZ in *Tg(gfap:GFP)mi2001* animals. We observed ependymoglial cells with radial morphology expressing both low and high GFP levels (arrow depicting GFP^high and arrowhead depicting the GFP^low in Figure 4A). Moreover, the FACS-based analysis of GFP levels in the *Tg(gfap:GFP)mi2001* transgenic line revealed two distinct GFP+ states based on the contour diagram plot in both intact and injured brains (Figure 4C). Cells from both states express comparable levels of typical ependymoglial markers such as Gfap, Nestin, and S100b, as detected by RT-qPCR performed on FACS-purified GFP+ cells (Figure 4D), therefore demonstrating the ependymoglial nature. However, the two ependymoglial states show different expression levels of other glial genes, such as Sox9b and Aromatase B, suggesting that the transcriptomic signatures of cells belonging to different states are not completely identical (Figure 4D). Notably, an analysis of their transcriptomes revealed clear clustering according to the GFP expression levels (Figure S4A) and the enrichment of distinct biological processes (Figures S4B and S4C). The GFP^high state is enriched in processes linked to cell proliferation, while processes related to cellular migration and differentiation are significantly enriched in the GFP^low state. However, these ependymoglial states are plastic with regard to GFP levels; some GFP^high cells achieved the GFP^low phenotype and vice versa within 5 days of *in vivo* live imaging in both intact and injured brains (Figure 4B). Nevertheless, 97% of all ependymoglia that directly convert into post-mitotic HuC/D+ neurons acquire the GFP^low phenotype before conversion (pink line in Figure 4B).

Therefore, we next set out to analyze the level of AhR signaling in the FACS-purified GFP^low population using the expression of AhR target gene Cyp1b1 as a readout. Importantly, we detected a downregulation of Cyp1b1, one of the major AhR targets, at 2 dpi in the GFP^low population that returns back to the intact brain basal levels at 7 dpi (Figure 4E). This regulation is parallel to the transcriptional upregulation of the Mcm7, Ccna2, and Nfkbie (Figures S4D–S4F) genes, showing inverse correlation to the activation state of AhR signaling (Marlowe et al., 2004). In contrast, these transcriptional changes could not be observed in GFP^high ependymoglia, with the exception of Nfkbie (Figures

S3A–S3C). In line with the regulation of AhR signaling targets, we further observed significantly higher levels of aryl hydrocarbon receptor 2 (ahr2) transcript in the GFP^low ependymoglia both in the intact and injured telencephalon (Figure S4G). Therefore, we performed RNA sequencing (RNA-seq) and compared the total transcriptomic changes in FACS-purified GFP^low ependymoglia at 1, 3, and 7 dpi to the intact brain. A multidimensional scaling plot showed a rapid reaction of GFP^low ependymoglia to injury with large differences in the overall transcriptomic signature already at 1 dpi (Figure S4H). The gene set enrichment analysis revealed AhR pathway (gene set defined based on the Ingenuity database) regulation in GFP^low ependymoglia at 1 and 3 days after injury compared to the intact brain, but not at 7 dpi (Figure 4F), in line with our Cyp1b1-based monitoring of signaling activity (Figure 4E). Moreover, we identified a significant downregulation (false discovery rate [FDR] < 0.05) of 3 pathways immediately after injury (1 dpi), including epithelial-mesenchymal transition (EMT) (Figure S4I), a process already linked to the level of AhR signaling (Rico-Leo et al., 2013). Therefore, these data suggest that the AhR-regulated EMT process could control the direct conversion of ependymoglia into the post-mitotic neurons during the repair process. Interestingly, the GFP^low population of ependymoglia specifically upregulates GATA3 (Figure S4J), a transcription factor implicated in restorative neurogenesis (Kyritsis et al., 2012), further corroborating the prime role of the GFP^low population in restorative neurogenesis. Notably, neurons generated by direct conversion are mostly susceptible to the AhR signaling levels, as we observed that these neurons fail to survive long term after precocious AhR activation (Figures 4G and 4H).

Taken together, we have identified a population of ependymoglial cells that generate new neurons in the zebrafish telencephalon by direct conversion and revealed the AhR signaling pathway that was thus far unknown in this context.

DISCUSSION

Brain injury in zebrafish induces a specific temporal sequence of cellular events starting with the accumulation of neutrophils and

---

Figure 4. AhR Signaling Is Regulated in the Population of Ependymoglia Undergoing Direct Conversion

(A) Micrograph with orthogonal projection and pixel intensity image depicting the surface of the ependymoglial cell layer in the Tg(*gfap:GFP*)*mi2001* line. The signal is obtained using *in vivo* imaging. Note that two different states of ependymoglia cells can be distinguished based on the following levels of GFP expression: GFP^high (arrow) and GFP^low (arrowhead).

(B) Lineage trees of ependymoglia cells undergoing direct conversion in the injured brains after AhR agonist or vehicle treatment. Every line in the box represents a single ependymoglia cell followed during the 5-day-period of *in vivo* imaging.

(C) FACS plots depicting the definition of the sorting gates (Brassy background) and sorting of gfap:GFP^high and GFP^low ependymoglia in intact and injured telencephalons based on the contour plots.

(D) Dot plot showing the real-time expression of glial genes in GFP^high- and GFP^low-sorted cells from intact brains. Single dots represent individual animals indicating biological replicates. Each biological replicate is the mean of 4 technical replicates. Lines show mean ± SEM. *p ≤ 0.05 (unpaired t test).

(E) Dot plot depicting the expression of Cyp1b1 in GFP^low ependymoglia-sorted cells from intact brains and after injury. Single dots represent individual animals indicating biological replicates. Each biological replicate is the mean of 4 technical replicates. Lines show mean ± SEM. *p ≤ 0.05 (repeated one-way ANOVA with Bonferroni post hoc test).

(F) Gene set enrichment analysis (GSEA) plot depicting AhR pathway regulation at 1, 3, and 7 days after injury in the GFP^low ependymoglial subpopulation.

(G) Micrographs with orthogonal projections depicting HuC/D and TdTomatomem double-positive cells negative for BrdU lacking radial morphology in AhR agonist- or vehicle-treated brains 5 days after injury. Images are presented as full z-projections of the confocal z stack.

(H) Dot plot showing the percentage of neurons generated by direct conversion (double-positive HuC/D and TdTomatomem cells negative for BrdU) among all TdTomatomem-positive cells after treatment with AhR agonist or vehicle at 5 dpi (short term) and 14 dpi (long term). Single dots represent individual animals indicating biological replicates. Lines show mean ± SEM. *p ≤ 0.05 (Mann-Whitney test).

DC, direct conversion; NES, normalized enrichment score.

microglia at the injury site. This accumulation is followed by the activation of oligodendrocyte progenitors within the first 24 hr after injury. Interestingly, the ependymoglial cells generating new neurons are fully activated somewhat later (Baumgart et al., 2012; Kroehne et al., 2011). This indicates an indirect activation of the ependymoglial cells. Notably, monocyte invasion and inflammation have been shown to be necessary for the activation of ependymoglia in zebrafish (Kyritsis et al., 2012) to generate long-term surviving neurons. The transcriptome analysis presented here further supports a role of immune cells in regulating neurogenesis, as we observed a number of pathways involved in the immune cell reaction to be specifically upregulated shortly after brain injury. However, most of these changes chase out toward 7 days after injury despite the significant increase in the proliferation of ependymoglial cells at this time point. These data suggest a paradigm in which initial changes in AhR levels prevent the premature engagement of ependymoglia cells primed to directly convert during the initial inflammatory phase. Notably, we were able to show that the interference with this timing by precociously activating AhR signaling leads to aberrant neurogenesis because additional new neurons generated in these conditions fail to survive. As ongoing inflammatory processes and astrogliosis prevent the survival and full differentiation of adult neural stem cell progeny in the mammalian brain after stroke (Dimou and Götz, 2014), our data raise the possibility that the mammalian central nervous system lost the capacity to precisely time the generation of new neurons and, therefore, regeneration capacity. The implementation of such a regulatory system in the injured mammalian brain might be the key to achieve successful regeneration.

Our analysis suggests that the appropriate regulation of AhR signaling after injury is necessary for the proper timing of restorative neurogenesis relative to the inflammatory phase of regeneration. The inhibition of AhR shortly after injury blocks the direct conversion of ependymoglia into neurons, while high levels of AhR achieved at 7 dpi promote direct conversion. The activity of the AhR pathway is controlled by a number of environmental factors including dioxins, polychlorinated biphenyls, polycyclic aromatic hydrocarbons (Stanford et al., 2016), tryptophan metabolites, and the cytokine network, suggesting a role of AhR signaling in sensing the environment after the injury. Indeed, the kynurenine pathway activated after traumatic brain injury (Yan et al., 2015) potentiates the AhR (Bersten et al., 2013), possibly via controlling tryptophan metabolism. The kynurenine pathway regulated in microglia in response to injury (Yan et al., 2015) could therefore provide endogenous ligands responsible for the translocation of AhR to the nucleus and could control the direct conversion in response to injury. The major AhR signaling mediator, AhR, is the nuclear receptor promoting the transcription of a spectrum of genes involved in the cell cycle, tissue homeostasis, early cell differentiation, and stress response (Bersten et al., 2013). The transcriptional activity of AhR is controlled by its shuffling between the nucleus and cytoplasm in a ligand-dependent manner (Bersten et al., 2013). Therefore, low AhR stability due to the PAS domain (Bersten et al., 2013) and ligand-dependent translocation to the nucleus allow the fast and dynamic AhR-mediated control of cellular behavior during wound healing and regenerative neurogenesis, including

direct conversion. Interestingly, adult neurogenesis in the dentate gyrus of the hippocampus influenced by activity is dependent on AhR signaling (Latchney et al., 2013). Moreover, AhR signaling regulates the differentiation of hematopoietic progenitors (Boitano et al., 2010), suggesting an emerging concept that AhR levels allow the synchronization of the current demands implied by the environment, such as injury and the stem cell output.

STAR★METHODS

Detailed methods are provided in the online version of this paper and include the following:

- KEY RESOURCES TABLE
- CONTACT FOR REAGENT AND RESOURCE SHARING
- EXPERIMENTAL MODEL AND SUBJECT DETAILS
  - Zebrafish lines
- METHOD DETAILS
  - Stab-wound injury
  - Plasmids
  - Plasmid electroporation and cerebroventricular micro-injections of drugs or morpholinos
  - *In vivo* imaging
  - Injected drugs
  - Morpholinos
  - Tissue preparation and immunohistochemistry
  - Laser capture microdissection
  - Microarray and Bioinformatics analysis
  - FACS sorting
  - RNA sequencing and Bioinformatic analysis
  - Real time q-PCR
  - BrdU labeling experiments
  - Cell death assay (TUNEL)
- QUANTIFICATION AND STATISTICAL ANALYSIS
  - Ependymoglia surface measuring (quantifications)
- DATA AND SOFTWARE AVAILABILITY
  - Software
  - Data

SUPPLEMENTAL INFORMATION

Supplemental Information includes four figures, two tables, and two videos and can be found with this article online at https://doi.org/10.1016/j.celrep.2018.11.055.

REFERENCES

Arvidsson, A., Collin, T., Kirik, D., Kokaia, Z., and Lindvall, O. (2002). Neuronal replacement from endogenous precursors in the adult brain after stroke. Nat. Med. 8, 963–970.

Barbosa, J.S., Sanchez-Gonzalez, R., Di Giaimo, R., Baumgart, E.V., Theis, F.J., Götz, M., and Ninkovic, J. (2015). Neurodevelopment. Live imaging of adult neural stem cell behavior in the intact and injured zebrafish brain. Science 348, 789–793.

Barbosa, J.S., Di Giaimo, R., Götz, M., and Ninkovic, J. (2016). Single-cell in vivo imaging of adult neural stem cells in the zebrafish telencephalon. Nat. Protoc. 11, 1360–1370.

Baumgart, E.V., Barbosa, J.S., Bally-Cuif, L., Götz, M., and Ninkovic, J. (2012). Stab wound injury of the zebrafish telencephalon: a model for comparative analysis of reactive gliosis. Glia 60, 343–357.

Becker, C.G., and Becker, T. (2015). Neuronal regeneration from ependymoradial glial cells: cook, little pot, cook!. Dev. Cell 32, 516–527.

Bello, S.M., Heideman, W., and Peterson, R.E. (2004). 2,3,7,8-Tetrachlorodibenzo-p-dioxin inhibits regression of the common cardinal vein in developing zebrafish. Toxicol. Sci. 78, 258–266.

Berghard, A., Gradin, K., and Toftgård, R. (1992). The stability of dioxin-receptor ligands influences cytochrome P450IA1 expression in human keratinocytes. Carcinogenesis 13, 651–655.

Bernardos, R.L., and Raymond, P.A. (2006). GFAP transgenic zebrafish. Gene Expr. Patterns 6, 1007–1013.

Bersten, D.C., Sullivan, A.E., Peet, D.J., and Whitelaw, M.L. (2013). bHLH-PAS proteins in cancer. Nat. Rev. Cancer 13, 827–841.

Boitano, A.E., Wang, J., Romeo, R., Bouchez, L.C., Parker, A.E., Sutton, S.E., Walker, J.R., Flaveny, C.A., Perdew, G.H., Denison, M.S., et al. (2010). Aryl hydrocarbon receptor antagonists promote the expansion of human hematopoietic stem cells. Science 329, 1345–1348.

Brill, M.S., Ninkovic, J., Winpenny, E., Hodge, R.D., Ozen, I., Yang, R., Lepier, A., Gascón, S., Erdelyi, F., Szabo, G., et al. (2009). Adult generation of glutamatergic olfactory bulb interneurons. Nat. Neurosci. 12, 1524–1533.

Chen, J., Magavi, S.S.P., and Macklis, J.D. (2004). Neurogenesis of corticospinal motor neurons extending spinal projections in adult mice. Proc. Natl. Acad. Sci. USA 101, 16357–16362.

Dimou, L., and Götz, M. (2014). Glial cells as progenitors and stem cells: new roles in the healthy and diseased brain. Physiol. Rev. 94, 709–737.

Dobin, A., Davis, C.A., Schlesinger, F., Drenkow, J., Zaleski, C., Jha, S., Batut, P., Chaisson, M., and Gingeras, T.R. (2013). STAR: ultrafast universal RNA-seq aligner. Bioinformatics 29, 15–21.

Ernst, A., Alkass, K., Bernard, S., Salehpour, M., Perl, S., Tisdale, J., Possnert, G., Druid, H., and Frisén, J. (2014). Neurogenesis in the striatum of the adult human brain. Cell 156, 1072–1083.

Fischer, J., Beckervordersandforth, R., Tripathi, P., Steiner-Mezzadri, A., Ninkovic, J., and Götz, M. (2011). Prospective isolation of adult neural stem cells from the mouse subependymal zone. Nat. Protoc. 6, 1981–1989.

Hestermann, E.V., and Brown, M. (2003). Agonist and chemopreventative ligands induce differential transcriptional cofactor recruitment by aryl hydrocarbon receptor. Mol. Cell. Biol. 23, 7920–7925.

Huber, A.B., Kania, A., Tran, T.S., Gu, C., De Marco Garcia, N., Lieberam, I., Johnson, D., Jessell, T.M., Ginty, D.D., and Kolodkin, A.L. (2005). Distinct roles for secreted semaphorin signaling in spinal motor axon guidance. Neuron 48, 949–964.

Kelsh, R.N., Brand, M., Jiang, Y.J., Heisenberg, C.P., Lin, S., Haffter, P., Odenthal, J., Mullins, M.C., van Eeden, F.J., Furutani-Seiki, M., et al. (1996). Zebrafish pigmentation mutations and the processes of neural crest development. Development 123, 369–389.

Kishimoto, N., Shimizu, K., and Sawamoto, K. (2012). Neuronal regeneration in a zebrafish model of adult brain injury. Dis. Model. Mech. 5, 200–209.

Kroehne, V., Freudenreich, D., Hans, S., Kaslin, J., and Brand, M. (2011). Regeneration of the adult zebrafish brain from neurogenic radial glia-type progenitors. Development 138, 4831–4841.

Kyritsis, N., Kizil, C., Zocher, S., Kroehne, V., Kaslin, J., Freudenreich, D., Iltzsche, A., and Brand, M. (2012). Acute inflammation initiates the regenerative response in the adult zebrafish brain. Science 338, 1353–1356.

Latchney, S.E., Hein, A.M., O'Banion, M.K., DiCicco-Bloom, E., and Opanashuk, L.A. (2013). Deletion or activation of the aryl hydrocarbon receptor alters adult hippocampal neurogenesis and contextual fear memory. J. Neurochem. 125, 430–445.

Livak, K.J., and Schmittgen, T.D. (2001). Analysis of relative gene expression data using real-time quantitative PCR and the 2(-Delta C(T)) Method. Methods 25, 402–408.

Love, M.I., Huber, W., and Anders, S. (2014). Moderated estimation of fold change and dispersion for RNA-seq data with DESeq2. Genome Biol. 15, 550.

Marlowe, J.L., Knudsen, E.S., Schwemberger, S., and Puga, A. (2004). The aryl hydrocarbon receptor displaces p300 from E2F-dependent promoters and represses S phase-specific gene expression. J. Biol. Chem. 279, 29013–29022.

McCurley, A.T., and Callard, G.V. (2008). Characterization of housekeeping genes in zebrafish: male-female differences and effects of tissue type, developmental stage and chemical treatment. BMC Mol. Biol. 9, 102.

Mootha, V.K., Lindgren, C.M., Eriksson, K.F., Subramanian, A., Sihag, S., Lehar, J., Puigserver, P., Carlsson, E., Ridderstrale, M., Laurila, E., et al. (2003). PGC-1alpha-responsive genes involved in oxidative phosphorylation are coordinately downregulated in human diabetes. Nat. Genet 34, 267–273.

Park, H.C., Kim, C.H., Bae, Y.K., Yeo, S.Y., Kim, S.H., Hong, S.K., Shin, J., Yoo, K.W., Hibi, M., Hirano, T., et al. (2000). Analysis of upstream elements in the HuC promoter leads to the establishment of transgenic zebrafish with fluorescent neurons. Dev. Biol. 227, 279–293.

Prasch, A.L., Teraoka, H., Carney, S.A., Dong, W., Hiraga, T., Stegeman, J.J., Heideman, W., and Peterson, R.E. (2003). Aryl hydrocarbon receptor 2 mediates 2,3,7,8-tetrachlorodibenzo-p-dioxin developmental toxicity in zebrafish. Toxicol. Sci. 76, 138–150.

R Development Core Team (2009). R: A Language and Environment for Statistical Computing (R Foundation for Statistical Computing).

Rainer, J., Sanchez-Cabo, F., Stocker, G., Sturn, A., and Trajanoski, Z. (2006). CARMAweb: comprehensive R- and bioconductor-based web service for microarray data analysis. Nucleic Acids Res. 34, W498–W503.

Rico-Leo, E.M., Alvarez-Barrientos, A., and Fernandez-Salguero, P.M. (2013). Dioxin receptor expression inhibits basal and transforming growth factor β-induced epithelial-to-mesenchymal transition. J. Biol. Chem. 288, 7841–7856.

Rothhammer, V., Mascanfroni, I.D., Bunse, L., Takenaka, M.C., Kenison, J.E., Mayo, L., Chao, C.C., Patel, B., Yan, R., Blain, M., et al. (2016). Type I interferons and microbial metabolites of tryptophan modulate astrocyte activity and central nervous system inflammation via the aryl hydrocarbon receptor. Nat. Med. *22*, 586–597.

Soshilov, A.A., and Denison, M.S. (2014). Ligand promiscuity of aryl hydrocarbon receptor agonists and antagonists revealed by site-directed mutagenesis. Mol. Cell. Biol. *34*, 1707–1719.

Stanford, E.A., Ramirez-Cardenas, A., Wang, Z., Novikov, O., Alamoud, K., Koutrakis, P., Mizgerd, J.P., Genco, C.A., Kukuruzinska, M., Monti, S., et al. (2016). Role for the Aryl Hydrocarbon Receptor and Diverse Ligands in Oral Squamous Cell Carcinoma Migration and Tumorigenesis. Mol. Cancer Res. *14*, 696–706.

Subramanian, A., Tamayo, P., Mootha, V.K., Mukherjee, S., Ebert, B.L., Gillette, M.A., Paulovich, A., Pomeroy, S.L., Golub, T.R., Lander, E.S., and Mesirov, J.P. (2005). Gene set enrichment analysis: a knowledge-based approach for interpreting genome-wide expression profiles. Proc. Natl. Acad. Sci. USA *102*, 15545–15550.

Xu, C., Volkery, S., and Siekmann, A.F. (2015). Intubation-based anesthesia for long-term time-lapse imaging of adult zebrafish. Nat. Protoc. *10*, 2064–2073.

Yan, E.B., Frugier, T., Lim, C.K., Heng, B., Sundaram, G., Tan, M., Rosenfeld, J.V., Walker, D.W., Guillemin, G.J., and Morganti-Kossmann, M.C. (2015). Activation of the kynurenine pathway and increased production of the excitotoxin quinolinic acid following traumatic brain injury in humans. J. Neuroinflammation *12*, 110.

STAR★METHODS

KEY RESOURCES TABLE

REAGENT or RESOURCE	SOURCE	IDENTIFIER
Antibodies		
Chicken Anti-Green Fluorescent Protein	Aves Labs	Cat# GFP_1020; RRID: AB_10000240
Rat Anti-BrdU	Abcam	Cat# ab6326; RRID: AB_305426
Rabbit Anti-Red Fluorescent Protein	Rockland	Cat# 600-401-379; RRID: AB_2209751
Rabbit Anti-HuC/HuD	Abcam	Cat# AB_210554; https://www.abcam.com/huchud-protein-antibody-ab210554.html
Mouse Anti-Human HuC/HuD neuronal protein	Molecular Probes	Cat# A-21271; RRID:AB_221448
Mouse Anti-FLAG M2 antibody	Sigma Aldrich	Cat# F1804-1MG
BABB clearing protocol	Huber et al., 2005	N/A
Chemicals, Peptides, and Recombinant Proteins		
β-naphthoflavone (BNF)	Sigma-Aldrich	Cat# N3633
AhR antagonist	Calbiochem	Cat# 182705
Dimethylsulfoxid (DMSO)	Sigma-Aldrich	CAS: 67-68-5
Fast Green FCF	Sigma-Aldrich	Cat# F258-25G
MS222	Sigma-Aldrich	Cat# A5040-25G
DAPI	Sigma Aldrich	Cat# 10236276001
BrdU	Sigma Aldrich	Cat# B5002
Aqua Poly/mount	Polysciences Inc	Cat# 18606-5
SYBR Green	QIAGEN	Cat# 204057
Critical Commercial Assays		
ApopTag Red *In Situ* Apoptosis Detection Kit	EMD Millipore	S7165
POL-membrane slides	Leica Microsystems	11505188
RNeasy Plus Micro Kit	QIAGEN	7404
Ovation Pico WTA System V2	NuGen	3302-12
Encore Biotin Module	NuGen	4200-12
Zebrafish 1.0 ST arrays	Affymetrix	902007
PicoPure RNA Isolation Kit	Thermo Fisher	KIT0204
SMART-Seq v4 Ultra Low Input RNA Kit	Clontech	634888
MicroPlex Library Preparation Kit v2	Diagenode	C05010012
Maxima first strand synthesis kit	Thermo Scientific	K1671
Deposited Data		
Microarray data	This study	GenBank: GSE102400
RNA-seq data	This study	GenBank: GSE121404
Experimental Models: Organisms/Strains		
Tg(gfap:gfp)mi2001	Bernardos and Raymond, 2006	ZFIN ID: ZDB-PUB-060616-45
Tg(HuC:GFP)	Park et al., 2000	ZFIN ID: ZDB-PUB-001205-14
Brassy	Kelsh et al.,1996	ZFIN ID: ZDB-PUB-970210-32

Continued

REAGENT or RESOURCE	SOURCE	IDENTIFIER
Oligonucleotides		
ahr2 Morpholino: MO-ahr2 TGTACCGAT ACCCGCCGACATGGTT	Gene Tools	Prasch et al., 2003
Morpholino: Standard control morpholino	Gene Tools	N/A
Primers for Real time qPCR see Table S2	This paper	N/A
Software and Algorithms		
ImageJ	National Institutes of Health	https://imagej.nih.gov/ij/
Fiji	Laboratory for Optical and Computational Instrumentation	https://fiji.sc/; RRID: SCR_002285
Imaris V 6.3 software	Bitplane	http://www.bitplane.com/
Imaris V 8.4.1 software	Bitplane	http://www.bitplane.com/
FW10-ASW software	Olympus	https://www.olympus-lifescience.com/en/support/downloads/#!dlOpen=%23detail847249651
GraphPad Prism 7	GraphPad Software	https://www.graphpad.com/
Expression console (v.1.2)	Thermofisher	https://www.thermofisher.com/us/en/home/life-science/microarray-analysis/microarray-analysis-instruments-software-services/microarray-analysis-software/affymetrix-expression-console-software.html
R Development Core	N/A	https://www.r-project.org
CARMAweb	N/A	https://carmaweb.genome.tugraz.at/carma/
Ensembl Genome browser 90	N/A	http://www.ensembl.org//useast.ensembl.org/index.html?redirectsrc=//www.ensembl.org%2Findex.html
QIAGEN's Ingenuity Pathway Analysis (IPA®)	QIAGEN	https://www.qiagenbioinformatics.com/
STAR	Dobin et al., 2013	https://github.com/alexdobin/STAR
DeSeq2	Love et al., 2014	https://bioconductor.org/packages/release/bioc/html/DESeq2.html
Gene Set Enrichment Analysis	Subramanian et al., 2005; Mootha et al., 2003	http://software.broadinstitute.org/gsea/index.jsp
Molecular Signatures Database	Subramanian et al., 2005	http://software.broadinstitute.org/gsea/msigdb/index.jsp

CONTACT FOR REAGENT AND RESOURCE SHARING

Further information and requests for resources and reagents should be directed to and will be fulfilled by the Lead Contact, Prof. Jovica Ninkovic (ninkovic@helmholtz-muenchen.de).

EXPERIMENTAL MODEL AND SUBJECT DETAILS

Zebrafish lines
Transgenic zebrafish lines that were used are *Tg(gfap:gfp)mi2001* (Bernardos and Raymond, 2006) and *Tg(HuC:GFP)* (Park et al., 2000) crossed with *brassy.* We also used non-transgenic strains AB/EK hybrid and *brassy* (Kelsh et al., 1996).

All experiments were done with 3-5 months old animals, as in this age range we do not observe any age-associated differences. Control and treated animals were littermates in individual experiments. We did at least 3 independent biological replicates in every experiment (the exact number of analyzed animals is specified in every dot plot) and analysis was done blindly.

All animals were kept under standard, husbandry conditions and experiments were performed according to the handling guidelines and regulations of EU and the Government of Upper Bavaria (AZ 55.2-1-54-2532-0916).

METHOD DETAILS

Stab-wound injury
Stab wound injury (nostril injury type) was performed in both telencephalic hemispheres as previously described (Baumgart et al., 2012). Stab-wound injuries were made using a 100 × 0.9 mm glass capillary needle (KG01, A. Hartenstein). All needles were pulled

on a Narishige Puller (model PC-10) using a ''One-stage'' pull setting at a heater level of 63.5°C. The resulting dimensions of the needle used to make the telencephalic injury were 5 mm in length and 0.1 mm in diameter.

Plasmids

For labeling of ependymoglia cells prior to imaging we used pCS2-TdTomatomem plasmid (Barbosa et al., 2015).

Constitutively active zebrafish AhR construct (caAhR) was cloned in-house. The N-terminal portion of zebrafish ahr2 lacking PAS B domain was amplified by PCR using zebrafish cDNA and was fused by Gibson cloning to the transactivation domain of mouse AhR obtained from mouse liver cDNA. In order to be able to follow caAhR *in vivo* the protein was tagged by a FLAG tag.

Plasmid electroporation and cerebroventricular microinjections of drugs or morpholinos

TdTomatomem plasmid DNA (2.5μg/μl) was diluted in distilled water (Aqua B. Braun) to the final concentration of 1 μg/μl and injected with the dye Fast Green (0.3 mg ml^{-1}; Sigma).

Fish were first anaesthetized in 0.02% MS222 and immobilized in a sponge. A small hole in the skull was made, in the region between the telencephalon and the optic tectum using a microknife (Fine Science Tools). Subsequently, ventricular injections of the plasmid DNA were performed as previously done (Barbosa et al., 2015) using a glass capillary (Harvard Apparatus) and a pressure injector (200hPa, Femtojet®, Eppendorf). Five electrical pulses (amplitude, 65 V; duration, 25 ms; intervals, 1 s) were delivered with a square-wave pulse generator TSS20 Ovodyne (Intracel) or using ECM830 square wave electroporator (BTX Harvard Apparatus).

In the case of CMVI only, we followed the same procedure as above described, however instead of plasmid DNA, drugs or morpholinos were diluted in artificial cerebro-spinal fluid (ACSF) and injected with the dye Fast Green (0.3 mg ml^{-1}; Sigma) in the ventricle using a glass capillary (Harvard Apparatus) and a pressure injector (170hPa, Femtojet®, Eppendorf).

After the electroporation or injection, fish were awakened in the aerated water and kept in their normal husbandry conditions until the first *in vivo* imaging session, FACS or immunohistochemical analysis.

In vivo imaging

For *in vivo* imaging we used only animals with the *brassy* background in order to minimize the interference of the auto-fluorescence from the pigment cells existing in wild-type strains.

Ependymoglia cells were labeled by electroporation (see above) of TdTomatomem plasmid and the first imaging session was made 4 days after electroporation in order to leave enough time for fluorescent protein expression and maturation. Subsequently, fish were imaged repetitively on the daily basis for 5 days. In order to facilitate the detection of fluorescent proteins, the skin above the telencephalon area was removed and the skull was thinned using a micro-driller (Foredom) before first imaging session as we have done previously (Barbosa et al., 2015). Fish were anesthetized using the MS222 concentrations described in Barbosa et al. (2015). 1x MS222 water was prepared by adding 4,2 mL of MS222 stock solution to 100ml of E3 medium. During imaging, fish were continuously intubated by delivering aerated 0.75x MS222 solution prepared based on Xu et al. (2015). After imaging sessions, fish were released from the holder and awakened in fresh aerated tank water to allow free swimming between imaging sessions in normal husbandry conditions (see above).

Imaging was performed with a multi-photon, near-infrared, pulsed MaiTai HP DeepSee laser, tunable from 690nm to 1020nm (Spectra Physics) and a FV10-MRG filter (barrier filter = 495– 540 nm, dichromatic mirror = 570 nm, BA 575–630 nm). A water immersion objective (XL Plan N, 25x, 1.05NA, Olympus) was used as in Barbosa et al.,2015. An excitation wavelength of 1005nm was used to excite simultaneously GFP and Tdtomato fluorophores. Images were acquired using the FW10-ASW 4.0 software (Olympus) with independent laser adjustments for each channel.

The *z*-brightness function was used to adjust laser intensity and detector sensitivity with depth, allowing image capture without changes in brightness. The optical sections were acquired with a resolution in the *x-y* dimension 800 × 800 pixels and in the *z*-dimension at 1,5 or 2 μm interval between single optical sections. The imaged area in each fish was reliably reidentified based on the distribution pattern of electroporated cells.

After the imaging, image analysis was performed using the ImageJ (Fiji) and Imaris V8.4 software (Bitplane). In case that the imaging was performed in the *Tg(gfap:GFP)mi2001* transgenic line, cells with the cell body residing on the surface of the telencephalon, radial process and *gfap*:GFP expression were identified as ependymoglia cells and only these cells were analyzed throughout the 5 day-time course.

In the case of imaging performed in *Tg(HuC:GFP)* transgenic line, ependymoglia cells were identified based on radial morphology. Non-glial cells derived from ependymoglia cells that upregulate HuC/D neuronal marker were classified as HuC/D-positive neurons.

Post-imaging analysis was done using BABB clearing protocol for post-imaging immunohistochemistry for confirmation of the identity of the imaged cells as previously described (Barbosa et al., 2016).

Injected drugs

β-naphthoflavone (BNF, Sigma Cat. N3633) was dissolved in DMSO at the concentration of 20mM. For CMVI it was diluted 1:100 in Artificial Cerebro-Spinal Fluid (ACSF, final concentration 20μM). DMSO used in control experiment (Vehicle) was diluted 1:100 in ACSF.

AhR antagonist (Calbiochem, Cat. 182705) was dissolved in DMSO at the concentration of 3mM. For CMVI it was diluted 1:500 in ACSF (final concentration 6μM). DMSO used in control experiment (Vehicle) was diluted 1:500 in ACSF.

Morpholinos

Zebrafish ahr2 morpholino was designed according to Prasch et al. (2003) and was obtained from Gene Tools (USA). The control morpholino was the standard control morpholino (Gene Tools, USA). Both ahr2-MO and Ctrl-MO were dissolved in sterile water at the concentration of 1mM. Prior to CMVI, they were diluted to final concentration of 0.5 mM in ACSF.

Tissue preparation and immunohistochemistry

Animals were sacrificed by MS222 overdose of tricaine methane sulfonate (MS222, 0,2%) by prolonged immersion. Tissue processing was performed as described previously (Baumgart et al., 2012).

Laser capture microdissection

Telencephalon was dissected from intact and injured brains (2 and 7 days after injury) of animals from the *Tg(gfap:gfp)mi2001* transgenic line. 30 μm thick coronal sections were obtained with a cryostat, mounted on POL-membrane slides, and frozen at −80°C until further processing. Sections were dehydrated by immersion in 75%EtOH for 1.5 minutes, then in 90%EtOH for 1.5 minutes, and finally in 100%EtOH for 2 minutes, dried briefly and immediately used for microdissections with Laser Capture Microscopy system (LMD6000, Leica, Germany). Microdissected areas: dorsal and intermediate subventricular zone (VZ, 50 μm width from the ventricular surface), and the brain parenchyma (DP) avoiding regions close to the injury site. The areas chosen for dissection were cut and catapulted to a collecting tube. VZ and DP areas coming from different sections were collected together for a total collected area ranging from 3×10^5 to 1×10^6 μm2 for each sample and immediately lysed in RTL buffer from the RNeasy Plus Micro Kit for RNA was extraction. RNA was extracted using the RNeasy Plus Micro Kit according to manufacturer instructions. The Agilent 2100 Bioanalyzer was used to assess RNA quality and only high-quality RNA (RIN $\geq$ 8) was further processed for microarray analysis.

Microarray and Bioinformatics analysis

1 ng total RNA was amplified using the Ovation Pico WTA System V2 in combination with the Encore Biotin Module. Amplified cDNA was hybridized on Zebrafish 1.0 ST arrays. Staining and scanning (GeneChip Scanner 3000 7G) were done according to the Affymetrix expression protocol including minor modifications as suggested in the Encore Biotion protocol. Expression console (v.1.2) was used for quality control and to obtain annotated normalized RNA gene-level data (standard settings including median polish and sketch-quantile normalization). Statistical analyses were performed by utilizing the statistical programming environment R (R Development Core Team, 2009) implemented in CARMAweb (Rainer et al., 2006). Genewise testing for differential expression was done employing the limma t test and probe sets with p < 0.05, fold-change > 1.5x and average expression in at least one group per brain region > 10. The genomic positions of all probe sets in the zebrafish microarray were extracted from Affymetrix website (http://www.affymetrix.com/analysis/inex.affx) by applying a Batch Query on the GeneChip Array "Zebrafish Gene 1.x ST" (genome version Zv9, 2011). Zebrafish gene identifiers were derived from Ensembl database by using a custom-written Perl script and the extracted genomic positions of the probe sets, via the Application Programming Interface (API), version 64. Subsequently homologous mouse genes were retrieved by Ensembl Compara database. The identified orthologs were then used for canonical pathway enrichment analyses through the use of QIAGEN's Ingenuity Pathway Analysis. Regulated gene sets as input were selected by filters for (to determine). From significantly enriched pathways (Fishers Exact Test, p < 0.05) relevant ones were manually selected.

FACS sorting

The dorsal telencephalon from the *Tg(gfap:gfp)mi2001* transgenic line was dissected from intact brains and 1, 2, 5, 7 and 10 days after injury. Telencephali coming from 2 animals were pulled in one tube before dissociation. A single cell suspension was prepared according to Fischer et al. (2011). Single cells were filtered through a 70μm cell strainer and centrifuged at 1500 rpm for 7 min. After this passage, 2 different procedures were used for intracellular FACS analysis of proliferating cells and FACS sorting of ependymoglial cells.

For FACS analysis of proliferating progenitors (PCNA+, gfap:GFP+ aNSCs), cells were fixed in 70% ice cold ethanol and analyzed according to Barbosa et al. (2015). PCNA staining was performed using anti-PCNA antibody (1:250) coupled with AlexaFluor647 donkey anti mouse IgG secondary antibody (1:800). FACS analysis was performed at a FACS Aria (BD) in BD FACS Flow TM medium. Debris and aggregated cells were gated out by forward scattersideward scatter; single cells were gated in by FSC-W/FSC-A. Gating for fluorophores was done using *brassy* animals for GFP gating and *Tg(gfap:gfp)mi2001* animals stained with secondary antibody only for PCNA staining. Different ependymoglial populations are identified by formation of two clear clusters of cells in contour plot and sorting gates are defined based on the contour plots.

For FACS sorting of ependymoglial GFP^low populations, cells were washed in PBS, centrifuged at 1500 rpm for 7 min, re-suspended in PBS and analyzed and sorted according to the gates. GFP gating was done using *brassy* animals. GFP low cells were sorted directly in Extraction Buffer from PicoPure RNA Isolation Kit. After 30 minutes incubation at 42°C, sample were kept at 80°C until further processing for RNA isolation for RNA sequencing or Real Time qPCR.

RNA sequencing and Bioinformatic analysis

Total RNA from FACS-sorted cells was isolated employing PicoPure RNA Isolation Kit including digestion of remaining genomic DNA according to producer's guidelines but final RNA elution was performed with nuclease-free water at 37°C. The Agilent 2100 Bioanalyzer was used to assess RNA quality and only high-quality RNA (RIN > 8) was further processed for cDNA synthesis with SMART-Seq v4 Ultra Low Input RNA Kit according to the manufacturer's instruction. cDNA was fragmented to an average size of 200-500 bp in a Covaris S220 device (5 min; 4°C; PP 175; DF 10; CB 200). Fragmented cDNA was used as input for library preparation with MicroPlex Library Preparation Kit v2 and processed according to the manufacturer's instruction. Deep sequencing was performed on Illumina HiSeq system with 50bp paired-end reads.

FASTQ files were mapped to the Danio rerio genome (danrer10) using STAR (Dobin et al., 2013) with default parameters. Raw read counts were normalized using DeSeq2 (Love et al., 2014) to calculate differential gene expression and to perform the PCA analysis. Genes were ranked according to the log fold change between two conditions. Gene Set Enrichment Analysis (Subramanian et al., 2005) was performed using Hallmark gene sets of the Molecular Signatures Database (Subramanian et al., 2005). A custom gene set for Aryl Receptor Pathway was derived from Ingenuity (Aryl Hydrocarbon Receptor Signaling).

Real time q-PCR

Total RNA from FACS-sorted cells or dissected telencephali was isolated using PicoPure RNA Isolation Kit according to the manufacturer's instruction and genomic DNA was removed. The Agilent 2100 Bioanalyzer was used to assess RNA quality and only high-quality RNA (RIN $\geq$ 8) was further processed for cDNA synthesis. cDNA synthesis was performed using random primers with the Maxima first strand synthesis kit. qRT-PCR was conducted using SYBR Green and a Thermo Fisher Quant Studio 6 machine. The expression of each gene was analyzed in triplicate. Data were processed with the $\Delta\Delta$Ct method (Livak and Schmittgen, 2001). Elf1a was used as a reference gene (McCurley and Callard, 2008). Quantification was performed on three independent samples. Primers are used for the Real Time qPCR are listed in Table S2.

BrdU labeling experiments

BrdU (10mM, Sigma) was used and fish were kept in BrdU containing aerated water for 22 h/day for 5 days. During the 2 hours outside of BrdU water, fish were kept in fresh water and fed. After the treatment, animals were divided in two experimental groups. One group of animals was sacrificed right after the BrdU treatment (5 days BrdU, short term neurogenesis experiment). The second group of animals was sacrificed 9 days after (5 days BrdU + 9 days chase, long term neurogenesis experiment).

Cell death assay (TUNEL)

To assess cell death, we used the ApopTag Red *In Situ* Apoptosis Detection Kit (Merck Millipore, S7165) following user manual.

QUANTIFICATION AND STATISTICAL ANALYSIS

Statistical analyses were performed with GraphPad Prism 7 software by using two-tailed unpaired t test for experiments with normal data distribution and Mann-Whitney if we could not determine the normal data distribution. Statistical tests are indicated in the figure legends. Data are presented as the mean ± standard error of the mean (SEM). Statistical parameters are reported in the respective figures and figure legends.

We did at least 3 repetitions of each experiment and analysis was done blindly.

Ependymoglia surface measuring (quantifications)

Quantification of the ependymoglia-free surface was done in Imaris V8.4 (Bitplane) and ImageJ (Fiji) software. The brains were prepared as whole mount and the measuring was done on the single brain hemispheres. First, surface rendering of each hemisphere of the telencephalon was done using Imaris software applying the same criteria to every sample. Afterward, the obtained surface image was imported in ImageJ and the free area was assessed using threshold analysis. Data are presented as the mean ± standard error of the mean (SEM). Statistical analysis was done using Mann-Whitney test as indicated throughout the manuscript.

DATA AND SOFTWARE AVAILABILITY

Software

All software is freely or commercially available and is listed in the STAR Methods description and Key Resources Table.

Data

The accession number for microarray data is GSE102400 and RNA-seq data GSE121404.